ACS chemical biology

Articles

pubs.acs.org/acschemicalbiology

Transformation of the Non-Selective Aminocyclohexanol-Based Hsp90 Inhibitor into a Grp94-Seletive Scaffold

Sanket J. Mishra,[†] Suman Ghosh,[†] Andrew R. Stothert,[‡] Chad A. Dickey,[‡] and Brian S. J. Blagg*[,†]

[†]Department of Medicinal Chemistry, The University of Kansas, Lawrence, Kansas, United States

[‡]Department of Molecular Medicine and Byrd Alzheimer's Research Institute, University of South Florida, Tampa, Florida 33613, United States

Supporting Information

ABSTRACT: Glucose regulated protein 94 kDa, Grp94, is the endoplasmic reticulum (ER) localized isoform of heat shock protein 90 (Hsp90) that is responsible for the trafficking and maturation of toll-like receptors, immunoglobulins, and integrins. As a result, Grp94 has emerged as a therapeutic target to disrupt cellular communication, adhesion, and tumor proliferation, potentially with fewer side effects compared to *pan*-inhibitors of all Hsp90 isoforms. Although, the N-terminal ATP binding site is highly conserved among all four Hsp90 isoforms, recent cocrystal structures of Grp94 have revealed subtle differences between Grp94 and other Hsp90 isoforms that has been exploited for the development of Grp94-selective inhibitors. In the current study, a structure-based approach has been applied to a Grp94 nonselective compound, SNX 2112, which led to the development of **8j** (**ACO1**), a Grp94-selective inhibitor that manifests ∼440 nM affinity and >200-fold selectivity against cytosolic Hsp90 isoforms.

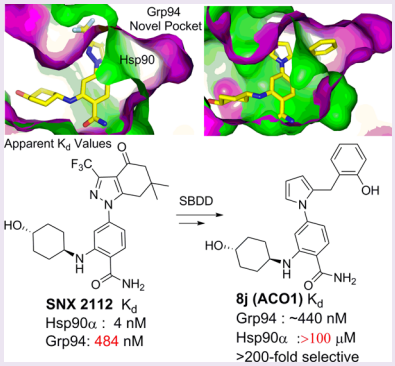

The heat shock protein 90 kDa (Hsp90) family of proteins is responsible for the conformational maturation of nascent polypeptides into their biologically active three-dimensional structures.[1] Hsp90 has generated great interest as a chemotherapeutic target due to its role in the modulation of cancer, neurodegenerative disorders, and infectious diseases. There are >200 protein substrates that require Hsp90 for their folding, maturation, and/or activation, termed Hsp90 clients.[2] During cellular stress, including elevated temperature, Hsp90 is induced to refold proteins that have undergone denaturation.[3,4] Similarly, Hsp90 is also upregulated in cancer cells, wherein it is required for the maturation of clients that drive the proliferation and growth of tumors.[4−7] Structurally, Hsp90 exists as a homodimer, and each monomer contains a C-terminus, N-terminus, and a highly charged middle domain. The N-terminus contains an ATP-binding site, which is responsible for ATP hydrolysis and provides the energy necessary for the folding of client protein substrates.[8,9]

Hsp90 exists as four isoforms: Hsp90α and Hsp90β reside in cytoplasm, whereas Grp94 localizes in the endoplasmic reticulum, and Trap1 is found in the mitochondria. The natural products, geldanamycin and radicicol, were among the first Hsp90 inhibitors identified and have served as useful tools to study Hsp90 biology, validating Hsp90 as a druggable target for the development of new anticancer agents.[10−12] Consequently, 17 Hsp90 inhibitors have entered clinical trials for the treatment of cancer, however, all of these compounds exhibit pan inhibition of all four Hsp90 isoforms.[13,14] Unfortunately, some Hsp90 inhibitors have manifested undesired activity during these investigations, which is likely to hinder subsequent evaluation. It has also been hypothesized that many of these side effects result from pan-inhibition of all four Hsp90 isoforms.[15] Therefore, the development of isoform-selective Hsp90 inhibitors can provide an opportunity to fine-tune the drug discovery process while simultaneously identifying isoform-dependent clients.

Glucose regulated protein 94 kDa (Grp94), also known as gp96 or endoplasmin, is the endoplasmic reticulum (ER) localized Hsp90 isoform. Grp94 is the most abundant protein in the ER lumen, where it is responsible for the maturation of secreted proteins that modulate immunity, cellular communication, and/or cell adhesion.[16] Grp94 is also a regulator of the unfolded protein response (UPR), a proteostatic mechanism triggered by the accumulation of misfolded proteins in the ER.[17,18] Client proteins that require Grp94 for their maturation include integrins, which are important for cell adhesion and metastasis, supporting Grp94 as a potential target for the development of antimetastatic agents.[19] Grp94 knockdown experiments in the highly metastatic breast cancer cell line, MDA-MB-231, and the reactive oxygen species (ROS) resistant MCF-7 cell line resulted in the inhibition of cell migration and metastasis.[20] In addition, myocilin represents another Grp94-dependent protein, which upon its aggregation leads to increased ocular pressure that results in primary open angle glaucoma (POAG), supporting Grp94 inhibition as a viable approach for the treatment of glaucoma.[21] Recently, maturation of the GARP and Wnt coreceptor, LRP6, was shown to be Grp94-dependent.[24] Since LRP6 is overexpressed in multiple

Received: August 25, 2016
Accepted: November 10, 2016

DOI: 10.1021/acschembio.6b00747
ACS Chem. Biol. XXXX, XXX, XXX−XXX

myeloma, Grp94 inhibition may be a useful for the treatment of such cancers.[22−24] As a consequence of these prior studies, the development of Grp94-selective inhibitors was sought for the treatment of various diseases, including cancer and glaucoma, while avoiding the potential side effects that result from inhibition of all four Hsp90 isoforms.

The N-terminal ATP-binding pocket of Grp94 is ∼85% identical to other Hsp90 isoforms, which presents a significant challenge for the design of isoform-selective inhibitors.[25] However, a five amino acid (QEDGQ) insertion into the Grp94 primary sequence results in a conformational change within the ATP-binding pocket that produces a small hydrophobic cleft that can be utilized to develop selective inhibitors.[26] Although, 5′-N-ethylcarboxamidoadenosine (NECA, Figure 1; **II**) was the first selective inhibitor of Grp94 identified, it manifests nonspecific agonistic activity against adenosine receptors.[27] However, the cocrystal structure of **II** bound to Grp94 revealed the ethyl amide to project into a small hydrophobic cleft within Grp94, which resulted in isoform-selective inhibition.[26] In an effort to identify other Grp94-selective inhibitors, radamide (RDA), a radicicol/geldanamycin chimeric inhibitor, was cocrystallized with both Grp94 and Hsp90 to probe binding interactions.[28] The cocrystal structure of RDA bound to Grp94 presented two modes of binding in which the amide bond existed in the *trans* or *cis* configuration, which was in contrast to the Hsp90 cocrystal structure, wherein the amide existed solely as the *trans* isomer. Upon further inspection, the structures suggested that the *cis*-amide selectively binds Grp94, whereas the *trans* isomer binds both homologues. Therefore, *cis*-amide bioisosteres of RDA were pursued and ultimately led to the discovery of BnIm (**III**),[30] which incorporates an imidazole ring in lieu of the *cis*-amide. Recently, Chiosis and co-workers reported another Grp94-selective inhibitor, PU-WS13 (**IV**), which binds to an alternative conformation of Grp94 than that reported for both **II** and RDA (Figure 2).[29]

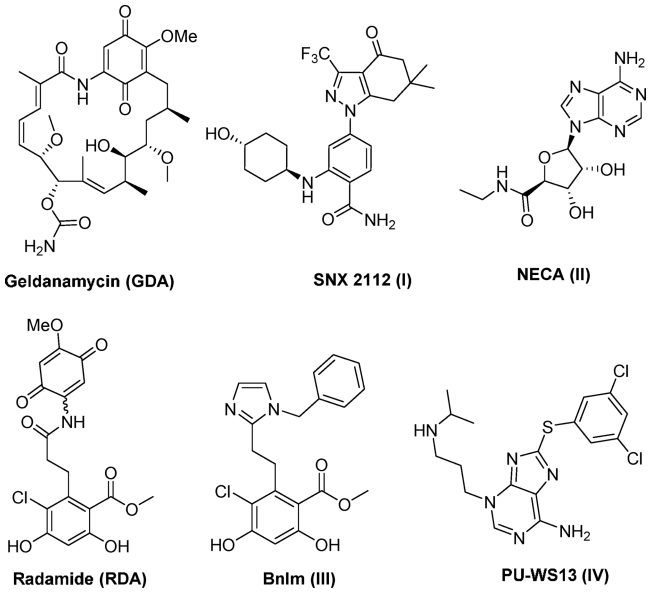

Figure 1. Structures of nonspecific Hsp90 inhibitors (GDA and SNX 2112) and Grp94-selective inhibitors (RDA, BnIm and PU-WS13, and NECA).

RATIONAL DESIGN

Upon examination of the binding modes for both **III** and **IV** bound to Grp94, it was revealed that Grp94 undergoes a conformational change when interacting with **IV** about helix 5 to form a binding pocket (site 2, Figure 2A) that is distinct from the structure of **III** bound to Grp94. The rotation about helix 5 brings Phe-195 in close proximity to the purine ligand and results in a closed conformation. Since the purine scaffold is not amenable to modifications that increase π interactions with Phe-195, a novel chemotype was designed to interact with Phe-195 while simultaneously accessing site 2. Recent work from our lab has explored the **II** binding pocket (Figure 2A) *via* derivatives of **III**;[30,31] however, access to site 2 remains underinvestigated. In an effort to design new analogs that provide access to these regions, the binding modes of Hsp90 inhibitors under clinical evaluation were investigated. In particular, SNX 2112 (**I**), a novel benzamide-containing compound was shown to bind both cytosolic Hsp90 isoforms (Hsp90 α/β K_d: 4/6 nM) with high affinity, but manifested lower affinity (Grp94 K_d: 484 nM) against Grp94 and TRAP1 (Figure 3A).[32]

Molecular modeling studies were then used to compare the binding mode of **I** with other scaffolds, including **III** and **IV**, which revealed **I** to occupy site 1 with the bulky tetrahydroindazolone fragment (Figure 3B). When bound to Hsp90, the tetrahydroindazolone fragment rotates and attains a near perpendicular geometry with the benzamide ring. Upon overlay of **I** bound to Hsp90 and **IV** bound to Grp94, it was observed that the tetrahydroindazolone fragment produces a steric clash in the closed conformation of Grp94 as illustrated in Figure 3C. In particular, the ketone, dimethyl, and trifluoromethyl groups of **I** appeared unable to bind the closed conformation of Grp94. Therefore, the tetrahydroindazolone fragment was computationally replaced with a pyrrole, which can also attain a coplanar geometry with the benzamide ring while simultaneously occupying site 2 to impart Grp94 selectivity. In fact, a substituted phenyl ring attached to the 2-position of the pyrrole appeared to preferentially bind the closed Grp94 conformation with high selectivity when compared to other Hsp90 isoforms (Figure 4). In addition, rotation of the pyrrole about the benzamide ring appeared to be disfavored as eclipsing interactions occur between the phenyl and aminocyclohexanol appendages (Figure 4A). The pyrrole also appeared to produce π interactions with Phe-195 in the Grp94 closed conformation (Figure 4B), and substitutions at the pyrrolic 2-position could lead to increased hydrogen bonding interactions with Asn-107, a residue that resides on the perimeter of the hydrophobic cleft. On the basis of these computational studies and observations, a new class of Grp94-selective inhibitors was synthesized and evaluated.

RESULTS AND DISCUSSION

Chemistry and Structure−Activity Relationship Studies. Synthesis of the proposed compounds began by treatment of pyrrole **1** with N-bromosuccinimide (NBS), followed by *in situ* protection of the nitrogen utilizing di-*tert*-butyl dicarbonate to form the corresponding N-boc-2-bromopyrrole, **2** (Scheme 1).[33,34] The brominated pyrrole (**2**) was then subjected to a Suzuki cross-coupling reaction with substituted aryl boronic acids using $Pd(dppf)Cl_2$ as a catalyst and potassium carbonate as the base. Subsequent removal of the Boc protecting group under basic conditions led to intermediates **3a−3j**.[35] Inter-

DOI: 10.1021/acschembio.6b00747
ACS Chem. Biol. XXXX, XXX, XXX−XXX

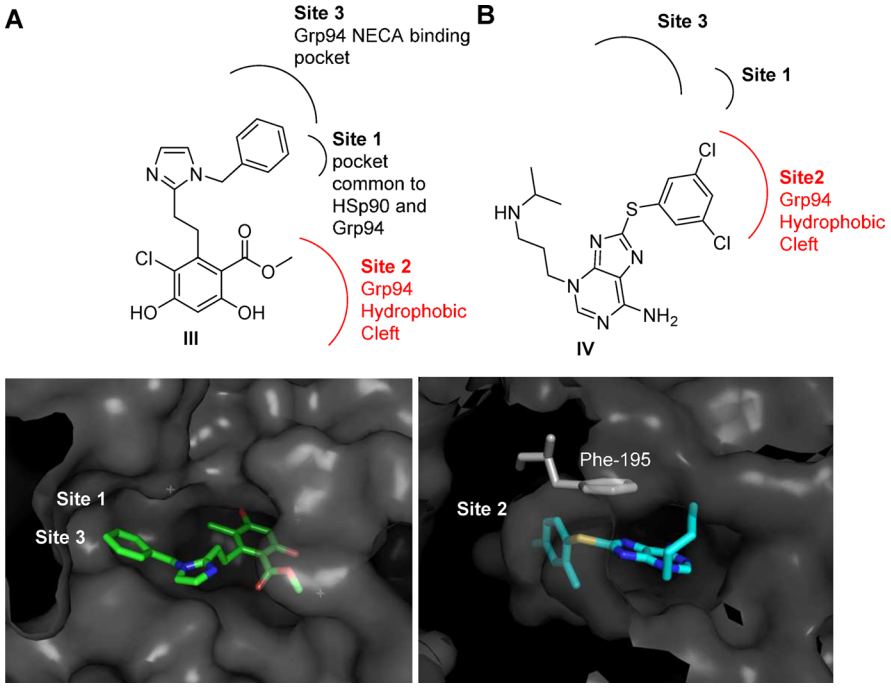

Figure 2. (A) Docking pose of **III** in Grp94 cocrystal structure with RDA (PDB code: 2GFD), showing **III** binding site 3 and site 1. (B) Binding pose of **IV** in Grp94 (PU-H54 in PDB code: 3O2F) in which the protein undergoes a conformational change and reveals site 2, bringing Phe-195 closer to the ligand. Site 3 and site 1 are not observed in this conformation.

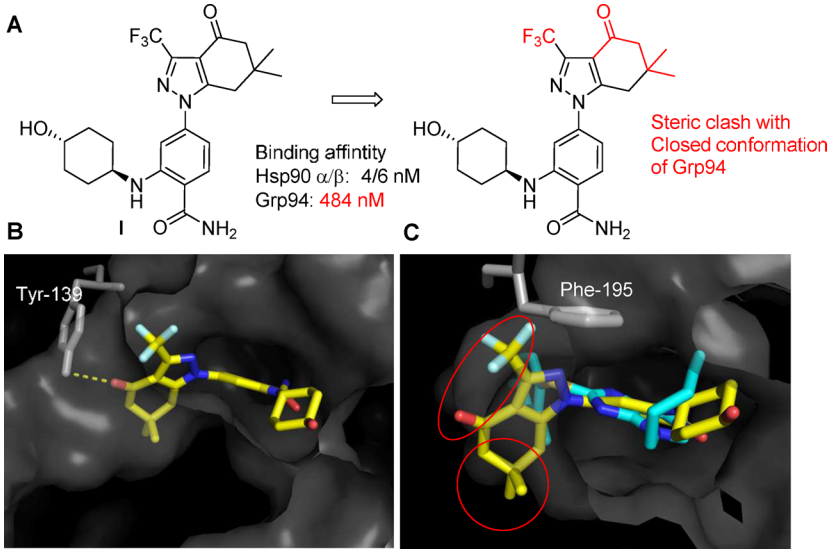

Figure 3. (A) **I** and its steric interactions with Grp94 (indicated in red). (B) **I** occupies site 1 when bound to Hsp90 (PDB code: 4NH7), establishing a hydrogen bond with Tyr-139, which might be lost during the conformational change of Grp94. (C) Overlay of the **I** Hsp90 binding mode with **IV** bound to Grp94. Steric clash manifested by **I** are depicted in red circles.

mediates **4a**–**4j** were obtained *via* a nucleophilic substitution reaction between **3a**–**3j** and 4-fluoro-2-bromobenzonitrile utilizing sodium hydride as the base in a solution of dimethylformamide. In the final step, amination of **4a**–**4j** was accomplished by microwave irradiation using *trans*-amino-cyclohexanol in the presence of potassium *tert*-butoxide and $Pd(OAc)_2$/DPPF. The crude material was then subjected to hydrolysis to convert the nitriles into the corresponding benzamides, **5a**–**5j**, in the presence of hydrogen peroxide and sodium hydroxide.

Compound **5a**, which contains an unsubstituted phenyl ring, was evaluated for binding affinity toward Grp94 and Hsp90. It was determined that compound **5a** bound Grp94 ($K_d \sim 9\ \mu M$) with greater affinity than Hsp90α ($K_d > 100\ \mu M$), supporting our hypothesis that these analogs represent a new class of Grp94-selective inhibitors (Figure 4B, Table 1). Following these encouraging results, structure–activity relationship (SAR) studies were explored for substituents on the phenyl ring to investigate both spatial and electronic requirements of the Grp94 binding pocket. The incorporation of methyl substituents onto the phenyl ring was pursued to explore steric demands at the 2-, 3-, and 4-positions (**5b**, **5c**, and **5d**). These compounds exhibited comparable affinity to **5a**, suggesting that additional space was available in this hydrophobic cleft.

DOI: 10.1021/acschembio.6b00747
ACS Chem. Biol. XXXX, XXX, XXX–XXX

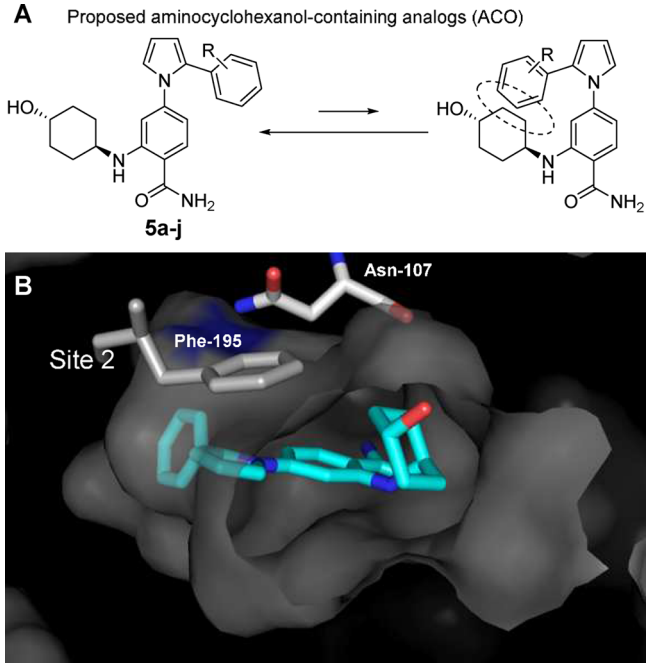

Figure 4. (A) Designed series of ACO inhibitors predicted to bind Grp94 in the desired conformation (left). (B) Docked pose of compound **5a** in the binding site of Grp94 in the closed conformation. The phenyl appendage at the 2-position of the pyrrole occupies site 2.

Scheme 1[a]

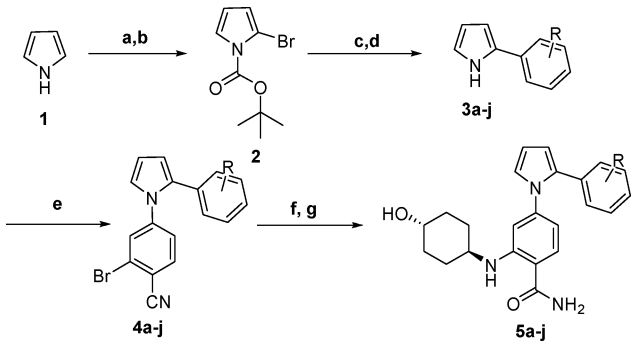

[a]Reagents and conditions: (a) NBS, −78 °C, THF. (b) TEA, DMAP, Boc_2O. (c) Pd(dppf)Cl_2, aryl boronic acid, toluene/ethanol/water (6:1:1), K_2CO_3,100 °C. (d) Methanol, K_2CO_3. (e) 4-Fluoro-2-bromobenzonitrile, NaH, DMF. (f) Pd$(OAc)_2$, DPPF, KO^{t}Bu, *trans*-cyclohexanolamine, MW, 110 °C. (g) DMSO, ethanol, NaOH, H_2O_2.

Subsequently, chlorine containing compounds (**5e**−**5g**) were synthesized to investigate the electronic effects within site 2. Both the 3- and 4-chloro substituted compounds (**5f** and **5g**) manifested decreased affinity; however, the 2-chloro derivative, **5e**, exhibited a K_d of ∼3 μM. The enhanced binding affinity exhibited by **5e** is not likely to result from steric effects, since the analog containing a methyl group (**5b**) at this location was less active. In addition, the phenyl ring in **5a** was replaced with a pyridine nitrogen at the 2-, 3-, and 4-positions (**5h**−**5j**) to explore the potential for hydrogen bonds with ASN107 (Figure 4). Unfortunately, 2- and 4-pyridine analogues resulted in decreased affinity for Grp94; however, **5i**, which contains a 3-pyridine ring, exhibited higher affinity than **5a**. Although **5i** did lead to increased affinity, it did not reflect strong interactions with Grp94 as supported by the computational studies, suggesting the pyridine nitrogen atom may not align properly

Table 1[a]

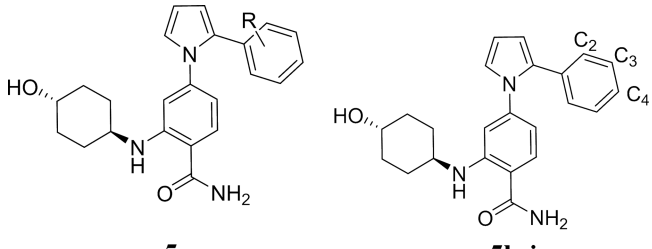

compound	R =	K_d, Grp94 (μM)	K_d, Hsp90α (μM)
5a	H	9.05 ± 0.31	> 100
5b	2-Me	9.9 ± 0.54	> 100
5c	3-Me	9.43 ± 0.26	> 100
5d	4-Me	8.35 ± 0.14	> 100
5e	2-Cl	2.94 ± 0.27	> 100
5f	3-Cl	15.8 ± 0.31	> 100
5g	4-Cl	10.62 ± 0.54	> 100
compound	N Scan	K_d, Grp94 (μM)	K_d, Hsp90α (μM)
5h	C_2 = N	13.98 ± 0.27	> 100
5i	C_3 = N	5.5 ± 0.15	> 100
5j	C_4 = N	13.2 ± 0.12	> 100

[a]Apparent K_d values determined using fluorescence polarization (FP) assay. Compounds were incubated with cGrp94/Hsp90α and FITC-GDA in triplicate, and ± SEM was measured.

in the binding site or that the rigidity of the scaffold may produce unfavorable steric interactions with the protein. In an effort to identify detrimental interactions within site 2, we performed additional molecular modeling studies that suggested the rigidity of the scaffold was detrimental to potency, as substituents at the 3-postion of the phenyl ring were too close to the Grp94 surface (Figure 4B). However, it appeared that a linker between the pyrrole and phenyl ring could provide the flexibility needed to overcome these unfavorable interactions, while projecting the phenyl ring deeper into the hydrophobic pocket (site 2).

Synthesis of the linker-containing compounds, **8** and **9**, is outlined in Scheme 2. The first synthetic process required preparation of the 2-benzylpyrrole fragments, **6a**−**6q**, *via* nucleophilic attack of the pyrrole onto the corresponding benzyl bromide/toluene sulfonate esters in the presence of methyl magnesium bromide. In the subsequent step, fragments **6a**−**6q** were subjected to the same sequence of reactions as required for the synthesis of **4a**−**4j** in Scheme 1. Toluene sulfonate esters **11a**−**11c** and **13** (Scheme 3) were prepared *via* a reaction between p-toluene sulfonyl chloride and the corresponding alcohols, which were utilized for the preparation of compounds **8j**−**8l** and **9**.

The two-carbon linker containing compound **9** appeared too long for accommodation in site 2, but was prepared to validate our binding model. Binding data confirmed that the benzyl substituted compound, **8a**, manifested greater affinity than the phenethyl derivative, **9** (Table 2). In fact, **8a** produced a K_d of ∼1.3 μM, an improvement over **5a**. Encouraged by the increased affinity and selectivity manifested by **8a**, SAR studies were initiated about the benzyl side chain *via* the incorporation of chlorine at all three locations on the phenyl ring, **8b**−**8d**. The 4-chloro derivative (**8d**) exhibited lower affinity for Grp94 than **8a**, suggesting limited space at the 4-position. Similarly, the 3-chloro analog, **8c**, also produced decreased affinity when

DOI: 10.1021/acschembio.6b00747
ACS Chem. Biol. XXXX, XXX, XXX−XXX

Scheme 2[a]

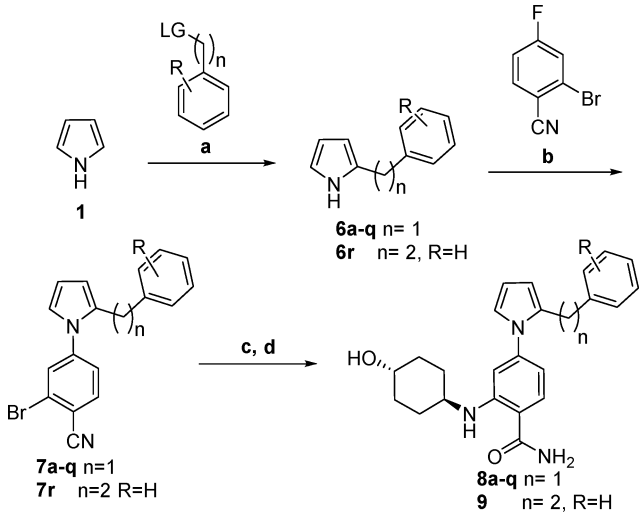

[a]Reagents and conditions: (a) MeMgBr, benzyl bromide/**11a−11c**/**13**, THF/DCM (1:1). (b) NaH, DMF. (c) $Pd(OAc)_2$, DPPF,KO^{t}Bu, *trans*-cyclohexanolamine, MW, 15 min, 110 °C. (d) DMSO, ethanol, NaOH, H_2O_2 RT (at 65 °C for **8j−8l**).

Scheme 3[a]

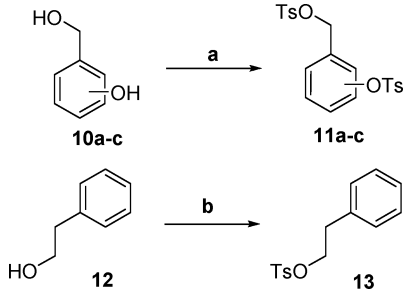

[a]Reagents and conditions: (a) NaH, TsCl (2.2 equiv), THF. (b) NaH, TsCl (1.1 equiv), THF.

Table 2[a]

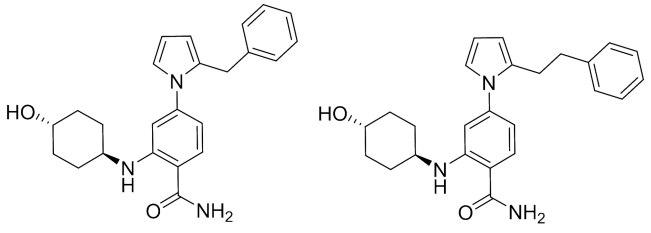

8a **9**

compound	K_d, Grp94 (μM)	K_d, Hsp90α (μM)
8a	1.13 ± 0.1	> 100
9	> 25	> 100

[a]Apparent K_d values determined using fluorescence polarization (FP) assay. Compounds were incubated with cGrp94/Hsp90α and FITC-GDA in triplicate and ± SEM were measured.

compared to **8a**. In contrast, the 2-chloro derivative, **8b**, produced increased affinity toward Grp94, while lacking affinity for Hsp90. Therefore, additional investigations at the 2-position were pursued. For this purpose, the 2-methyl substituted analog, **8i**, was synthesized, and upon evaluation, a loss of affinity was observed (~3 fold), suggesting that steric bulk at the 2-position was not tolerated. Therefore, substituents that exhibit various electronic features were incorporated into the 2-position (**8e−8g**). For example, the 2-fluorine analog, **8e**, resulted in improved affinity (~724 nM). However, the 3-fluorine (**8f**) and 4-fluorine (**8g**) analogs produced decreased affinity. Compound **8h** contained a bromide, but it too exhibited decreased affinity. On the basis of the data observed, we proposed that fluorine interacts with ASN107, which is also supported by prior studies that have demonstrated that the fluorine atom can interact with asparagine as a hydrogen bond acceptor.[36] Building on the knowledge that the 2-position of the benzyl ring is important for affinity and that ASN107 in Grp94 may produce hydrogen bonding interactions, phenol containing compounds, **8j−8l**, were synthesized. Upon their preparation, **8j−8l** were evaluated for binding affinity. Interestingly, the 2-phenol containing derivative **8j** exhibited an apparent K_d of ~446 nM toward Grp94 while maintaining >100 μM K_d for binding Hsp90 (>200 fold selectivity). The increased potency of compound **8j** could once again be explained *via* hydrogen bonding interactions with ASN107 *via* the phenol. Furthermore, the 3-phenol compound, **8k**, and the 4-phenol, **8l**, bound Grp94 with lower affinity (Table 3). The

Table 3[a]

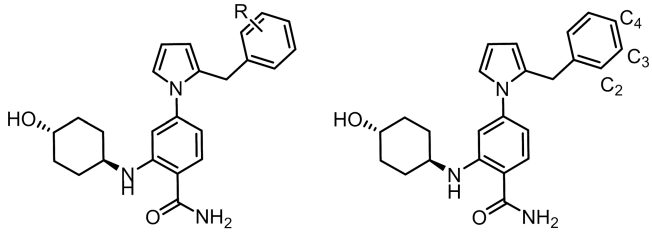

8b-n **8o-q**

compound	R =	K_d, Grp94 (μM)	K_d, Hsp90α (μM)
8b	2-Cl	0.83 ± 0.12	> 100
8c	3-Cl	2.45 ± 0.45	> 100
8d	4-Cl	> 25	> 100
8e	2-F	0.72 ± 0.14	> 100
8f	3-F	4.53 ± 0.12	> 100
8g	4-F	8.35 ± 0.14	> 100
8h	2-Br	12.9 ± 0.11	> 100
8i	2-Me	4.2 ± 0.23	> 100
8j	2-OH	0.44 ± 0.09	> 100
8k	3-OH	> 25	> 100
8l	4-OH	20.55 ± 0.74	> 100
8m	2-OMe	1.15 ± 0.02	> 100
8n	2, 6-di-F	> 25	> 100
compound	N scan	K_d, Grp94 (μM)	K_d, Hsp90α (μM)
8o	C_2 = N	13.98 ± 0.27	> 100
8p	C_3 = N	5.5 ± 0.15	> 100
8q	C_4 = N	13.2 ± 0.12	> 100

[a]Apparent K_d values determined using fluorescence polarization (FP) assay. Compounds were incubated with *c*Grp94/Hsp90α and FITC-GDA in triplicates and ± SEM were measured.

loss of affinity for the 3- and 4-phenols was in agreement with the affinities observed for substituents at the 3-and 4-positions. However, a hydroxyl group could serve as a hydrogen bond donor or an acceptor; therefore, the 2-methoxy containing compound, **8m**, was synthesized to differentiate the role of the 2-phenol with regard to ASN107. Compound **8m** bound Grp94

DOI: 10.1021/acschembio.6b00747
ACS Chem. Biol. XXXX, XXX, XXX−XXX

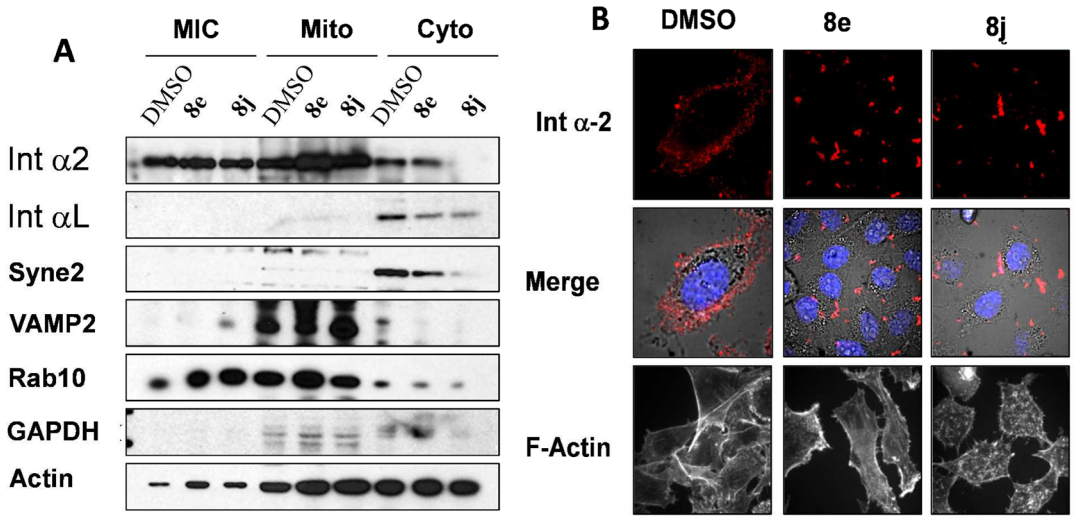

Figure 5. Biological evaluation of Grp94 inhibitors. (A) DMSO, **8e** (10 μM), and **8j** (10 μM) treated PC3-MM2 cells for 24 h were divided into microsomal (MIC), mitochondrial (Mito), and cytoplasmic (Cyto) fractions, and Western blot analysis was performed. Representative Western blots show the levels of integrin α2, integrin αL, Syne2, VAMP2, Rab10, and actin. (B) PC3-MM2 cells were treated with DMSO, **8e** (10 μM), or **8j** (10 μM) for 24 h and were fixed and stained with integrin α2 (red), phalloidin (gray), and DAPI (blue). Fluorescent images are representative of three independent biological replicates.

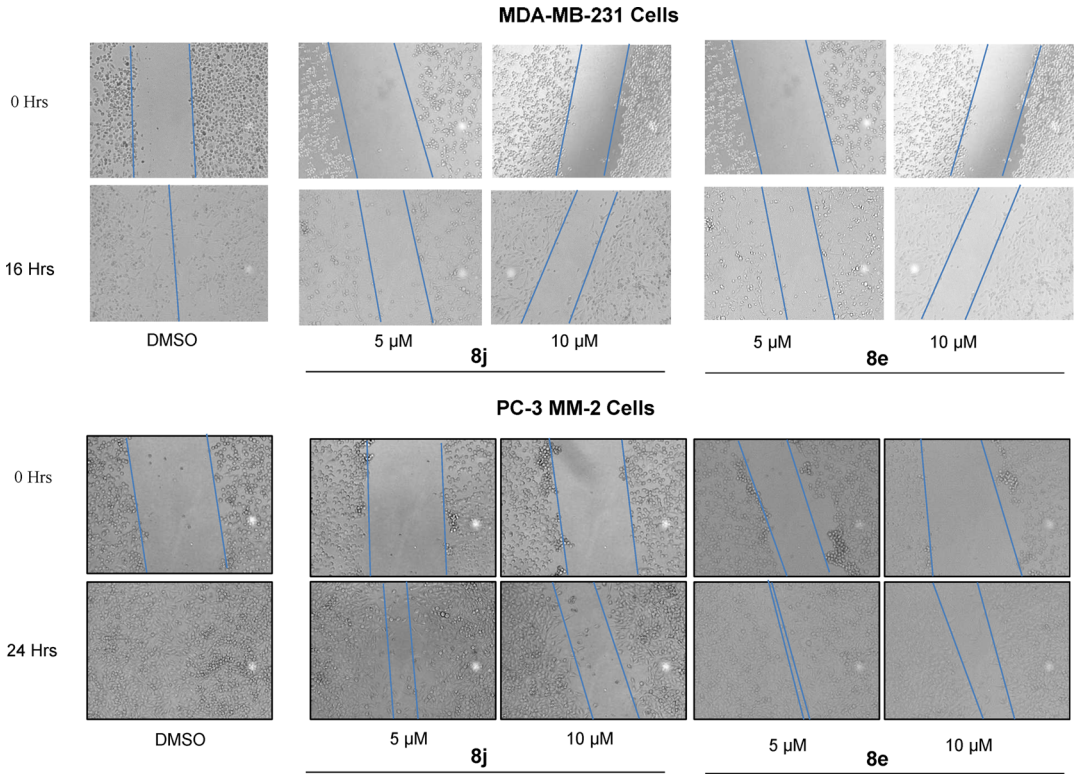

Figure 6. Wound-healing scratch assay performed with compound **8j** and **8e**. Top MDA-MB-231 cells and bottom PC-3 MM-2 cells. A camera mounted microscope was then used to record migration at 0, 16, and 24 h. Compounds **8j** and **8e** were evaluated in this assay at 10 μM and 5 μM concentration. Representative live cell images at the corresponding time points of three independent biological replicates of cell migration assay are shown.

with a K_d of 1.15 μM, which was comparable with **8a**, despite the hydrophobic constraints at the 2-position, which led us to conclude that the hydrogen bond acceptor role of the phenol is beneficial. Subsequently, the 2,6-difluorine substituted compound, **8n**, was synthesized to simultaneously occupy the binding pocket at both the 2- and 6-positions. Compound **8n** exhibited decreased affinity for Grp94, suggesting that the binding pockets surrounding the 2- and 6-positions are mutually exclusive (Figure 4). A nitrogen scan was also performed with compounds **8o**−**8q** to seek potential hydrogen bond interactions with protein, but a loss of binding affinity was observed compared to **8a**.

Grp94 Inhibitors Exhibit Antimigratory Activity. Grp94 is a pro-oncogenic chaperone that is overexpressed in tumors to

DOI: 10.1021/acschembio.6b00747
ACS Chem. Biol. XXXX, XXX, XXX−XXX

modulate cancer cell migration and metastasis.[37,38] Using Grp94 knockdown cells, it was reported that Grp94 affects intracellular transport pathways during the metastatic process. Although the total levels of proteins did not alter, levels in the microsomal fraction (MIC) were significantly lower in Grp94 knockdown cells compared to control cells, suggesting that Grp94 affects protein localization/trafficking. Specifically, Grp94 knockdown cells down-regulated VAMP2 and Rab10, which are critical for intracellular transport; Syne2, which is necessary for f-actin attachment to the nucleus; and integrin $\alpha 2$ and αL, which are critical for cell−cell and cell−matrix adhesion.[37] As shown in Figure 5A, the cytoplasmic (Cyto) fraction of cells treated with **8j** and to some extent **8e** at 30 μM resulted in reduced levels of integrin $\alpha 2$, integrin αL, Syne2, VAMP2, and Rab10 compared to DMSO, supporting that compound **8j** targets Grp94 more effectively than **8e**.

The cell migration process requires cell polarization, protrusion (filopodia, lamellipodia formation), adhesion, and retraction of the rear. Cell protrusion is produced by local actin polymerization causing filamentous actin (f-actin) formation at the filopodia and lamellipodia.[39] Adhesion is facilitated by formation of the focal adhesion complex at the filopodia tip. Focal adhesion occurs *via* integrin receptors that bind the extracellular matrix.[37] Different aspects of cell migration processes, such as f-actin localization and integrin trafficking, were therefore investigated by confocal microscopy using Grp94 inhibitors **8e** and **8j**. The microscopy data revealed that f-actin was enriched at the cellular cortex region in DMSO treated cells, which correlates with normal f-actin distribution. In the presence of **8j** and to some extent **8e**, f-actin formed sporadic patches in the cytoplasm, which further supported the role of Grp94 inhibitors to modulate cell protrusion *via* f-actin reorganization (Figure 5B).[40] Immunofluorescence analysis showed that integrin $\alpha 2$ is localized to the cell surface in untreated cells; however, in the presence of Grp94 inhibitors (**8e** and **8j**), integrin $\alpha 2$ was localized as patches in the cytoplasm, supporting the role of Grp94 to traffic integrins to the cell membrane (Figure 5B). As shown in Figure 6, Grp94 inhibitors, **8e** and **8j**, inhibited cell motility. When combined, these results show that both **8j** and to some extent **8e** prevent cancer cell migration by affecting f-actin polymerization and integrin trafficking and thus provide a clear mechanism by which Grp94 inhibitors inhibit the metastatic process. Recently, Grp94 inhibition was shown to diminish cell migration and metastasis in the highly metastatic breast cancer cell lines, MDA-MB-231 and ROS-resistant MCF-7.[20] The migratory activity of these cells was therefore determined by employing a wound healing scratch assay. It was observed that compounds **8j** and **8e** inhibited migration of the highly metastatic breast cancer cell line, MDA-MB-231, as well as the highly metastatic prostate cancer cell line, PC-3 MM-2, at 10 μM and 5 μM, respectively. The antiproliferative activity manifested by these compounds did not affect the proliferation of MDA-MB-231 or PC-3 MM-2 cells (>95% viability at 25 μM **8j** and **8e**), suggesting that the antimigratory activity manifested by these compounds does not result from antiproliferative activity. Taken together, the results show that these Grp94 inhibitors inhibit cell migration by disrupting integrin trafficking and filamentous actin rearrangement.

Disaggregation of Mutant Myocilin with Grp94 Inhibitors. Myocilin is a secreted protein found in trabecular meshwork (TM) tissue in the anterior anatomical segment of the eye. Gain of toxic function mutations in the MYOC gene lead to abnormal myocilin that readily accumulates and aggregates, leading to reduced aqueous humor outflow facility through the TM in the anterior chamber of the eye. As a result, intraocular pressure (IOP) is increased and contributes to primary open angle glaucoma (POAG), a degenerative eye disease.[41] Previous studies have found a link between the accumulation of aggregated mutant myocilin and the ER-associated chaperone, Grp94, and that the inhibition of Grp94 with small molecules is a viable therapeutic approach that can potentially lead to the alleviation of known POAG pathologies *via* increased clearance of myocilin aggregates from the ER.[21] Therefore, varying doses of inhibitors were evaluated in an assay that measured the levels of I477N mutant myocilin levels expressed in tetracycline inducible HEK cells that conditionally overexpress the I477N mutant form of myocilin. In the Western blot analysis shown in Figure 7, compound **8j** exhibited a significant decrease in mutatnt myocilin levels at 30 μM. Effect of drug on cytosolic Hsp90 client protein maturation was also determined. As can be seen in Figure 7b, compound **8j** did not affect Akt maturation at the evaluated concentration; Akt is a well-established Hsp90-dependent client. Furthermore, Hsp70 levels remained unaffected with **8j** when compared to 17-AAG, which is a pan-inhibitor of all four Hsp90 isoforms.

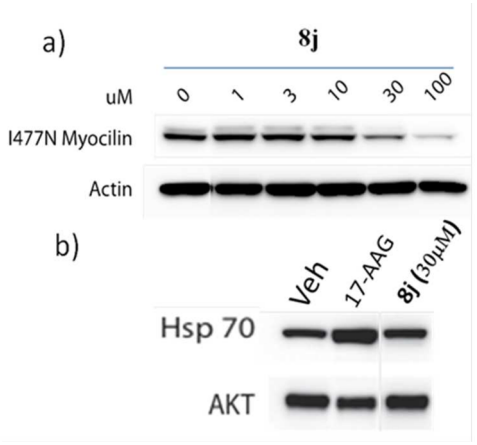

Figure 7. Western blot analysis of compound **8j** on the levels of (a) mutant myocilin and (b) Hsp70 and Akt with 30 μM **8j** and 5 μM of 17-AAG.

CONCLUSION

Herein, we report the discovery of a novel Grp94-selective scaffold that binds Grp94 in a conformation that is disfavored for binding other Hsp90 isoforms. The design and development of this new scaffold required the evaluation of existing inhibitors of the N-terminal ATP-binding site of Hsp90, which were screened *in silico* for their ability to bind the Grp94 hydrophobic cleft (site 2). It was determined that the benzamide-containing compound, SNX 2112 (**I**), could be modified to occupy the Grp94 hydrophobic cleft and could be used for the development of Grp94 selective inhibitors. For this purpose, the tetrahydroindazolone fragment of **I** was replaced with a pyrrole, and subsequent incorporation of a phenyl appendage led to **5a**, which exhibited good selectivity for Grp94 but lacked high affinity. Subsequent SAR studies led to analogs that incorporated a benzyl moiety in lieu of the phenyl and resulted in derivatives that exhibited both increased affinity and

DOI: 10.1021/acschembio.6b00747
ACS Chem. Biol. XXXX, XXX, XXX−XXX

selectivity. Additional investigations led to identification of **8j** (**ACO1**), which contains a phenol at the 2-position of the benzyl side chain. Biological investigations with **8j** determined that Grp94 was inhibited in cells and ultimately led to inhibition of cancer cell migration and induced the degradation of mutant myocilin. As a result, **8j** represents a new Grp94-selective inhibitor that may be useful for the treatment of metastatic cancer and/or glaucoma.

EXPERIMENTAL PROCEDURES

Chemistry. Synthetic procedures and full characterization of new compounds is provided in the Supporting Information.

Fluorescence Polarization. Assay buffer (25 μL, 20 mM HEPES at pH 7.3, 50 mM KCl, 5 mM $MgCl_2$, 1 mM DTT, 20 mM Na_2MoO_4, 0.01% NP-40, and 0.5 mg mL^{-1} BGG) was added to a 96-well plate (black well, black bottom) followed by the desired compound at the indicated final concentrations in DMSO (1% DMSO final concentration). Subsequently, 10 nM recombinant cGrp94/Hsp90α and 6 nM FITC-GDA were added in 50 and 25 μL assay buffer respectively, resulting in a 100 μL final volume. Plates were incubated for 5 h at 4 °C on a rocker. Fluorescence was determined using excitation and emission filters of 485 and 528 nm, respectively. Percent FITC-GDA bound was determined by assigning the DMSO millipolarization unit (mP) value as the 100% bound value and 0% for FITC-GDA in assay buffer without any protein. K_d values were calculated from separate experiments performed in triplicate using GraphPad Prism.

Molecular Modeling. The Surflex-Docking module in Sybyl v8.0 was used for molecular modeling and docking studies. The cocrystal structures of RDA bound to Grp94 (PDB code: 2GFD), SNX 2112 bound to Hsp90 (PDB code: 4NH7), and PU-H54 bound to Grp94 (PDB code: 3O2F) were utilized for modeling experiments. Pymol was used for further visualization and figure preparation.

Protein Trafficking and Anti-Migratory Effects of Grp94 Inhibitors. *Chemicals and Cell Culture.* Compounds **8e** and **8j** were dissolved in DMSO and stored at −20 °C. The PC3-MM2 and MDA-MB-231 cells were maintained in DMEM (Cellgro) media supplemented with streptomycin (500 μg/mL), penicillin (100 units/mL), and 10% FBS at 37 °C and 5% CO_2.

Antibodies. The following antibodies were used for Western blotting and/or immunofluorescence: goat anti-integrin αL #sc6609, rabbit anti-SYNE2 #sc99066, and rabbit antiactin #sc1616-R (Santa Cruz Biotechnology); rabbit anti-Integrin α 2 #ab181548 and rabbit anti-VAMP2 #ab3347 (Abcam); Phalloidin 647 #A22287 (Invitrogen); and rabbit anti-Rab10 #4262S (Cell Signaling Technology).

Cell Fractionation and Western Blot Analysis. The PC3-MM2 cells treated with DMSO, or compounds dissolved in DMSO at specified concentrations for 24 h, were trypsinized, washed twice with ice-cold phosphate-buffered saline (PBS), and resuspended in 10 mL of isolation buffer containing 10 mM Tris-HCl at pH 7.4, 1 mM EDTA, 0.2 M D-mannitol, 0.05 M sucrose, 0.5 mM sodium orthovanadate, 1 mM sodium fluoride, and protease inhibitor cocktail.[42] The cells were homogenized with the aid of a Teflon pestle, and lysis was confirmed microscopically. After sedimenting the cell debris, the protein concentration of each lysate was measured in quadruplicate using the BCA protein assay and bovine serum albumin as the standard. The coefficient of variation was determined for each set of quadruplicate measures, and if the variability exceeded 5%, the protein assay was repeated for that set of samples. The cell lysates containing equal amounts of protein were centrifuged at 8000*g* for 10 min, and the crude mitochondrial pellet (Mito) was washed two times in isolation buffer and frozen. The reserved supernatant was centrifued at 14 000*g* to isolate a microsomal fraction (MIC) and the remaining supernatant (Cyto) was concentrated overnight by TCA precipitation and dissolved in a minimum amount of isolation buffer and subjected to SDS-PAGE.

Equal volumes of samples were electrophoresed under reducing conditions (8% polyacrylamide gel), transferred to a polyvinylidene fluoride membrane (PVDF), and immunoblotted with the corresponding specific antibodies. Membranes were incubated with an appropriate horseradish peroxidase-labeled secondary antibody, developed with a chemiluminescent substrate and visualized.

Immunofluorescence Analysis. For cell imaging, 1 μm-Slide eight-well ibidiTreat IBIDI glass slides were used. PC3-MM2 cells were fixed with freshly made 4% (w/w) paraformaldehyde in PBS for 15 min, permeabilized with 0.1% (w/w) Tween 20 in PBS for 5 min, and quenched with 0.1% (w/w) sodium borohydride for 5 min. The sections were blocked with 3% (w/w) BSA in PBS for 1 h and incubated with the primary antibody at a 1:100 concentration in 1% BSA in PBS overnight, prior to incubation with secondary antibody conjugated with Alexa Fluor 568 for 3 h. The sections were counterstained with DAPI and/or with phalloidin to visualize DNA and F-actin, respectively. The wells were washed three times with PBS after each step.

Confocal images were acquired using a custom epifluorescent/confocal microscope composed of the following components: an Olympus IX81 inverted spinning disc confocal microscope base (Olympus America), a Prior microscope stage for automated image acquisition (Prior Scientific), an Olympus 60× oil immersion objective for confocal images, and a Hamamatsu Electron Multiplying Charge-Coupled Device (EMCCD) camera (Hamamatsu). Images were captured using the SlideBook acquisition and analysis software (Intelligent Imaging Innovations (3i)).

Images were collected with 8−10 image stacks with a 0.3 μm step size through the cells. Images were processed using ImageJ software (NIH).

Wound Healing Scratch Assay. The cells were seeded in a 24-well plate in complete media and allowed to form a monolayer. After monolayer formation, a scratch was introduced with a sterile 0.1−10 μL pipet tip. The medium was replaced with fresh medium in the absence or presence of the indicated drug concentrations. Photomicrographs were taken at different time points with an Olympus IX71 microscope using a 10× air lens and CellSans Dimensions software. The images were processed with ImageJ software.

Antiproliferation Assays. Cells were seeded (2000/well, 100 μL) in 96-well plates and incubated overnight. Following incubation, compounds with varying concentrations in DMSO (1% DMSO final concentration) were added, and cells were returned to the incubator for 72 h. After 72 h, the cell viability was determined using an MTS/PMS cell proliferation kit (Promega) per the manufacturer's instructions. Absorption values from 1% DMSO wells were used as 100% proliferation, and values were adjusted accordingly.

Effect of Grp94-Selective Inhibitors on Myocilin Levels. *Cell Culture.* Cell culture was performed as previously described.[21] Tetracycline-inducible Hek cells stably overexpressing I477N mutant myocilin were grown and maintained in Dulbecco's Modified Eagle's Medium supplemented with 10% fetal bovine serum (Invitrogen, penicillin (100 units/mL), streptomycin (100 mg mL^{-1}), and 1% GlutaMAX (Invitrogen) at 37 °C and 5% CO_2). Stably overexpressing cells were selected for using hygromycin B (200 mg mL^{-1}; InvivoGen) and G418 (100 mg mL^{-1}; Gibco). I477N myocilin expression was induced with tetracycline (5 mg mL^{-1}) for 48 h prior to drug treatment.

Inhibitor Treatment. Inhibitors were solubilized in DMSO (Sigma-Aldrich) and diluted to documented concentrations. Cells were treated dropwise with inhibitors 24 h prior to cell harvest. DMSO concentration was diluted to 1% total cell medium volume.

Cell Harvest. Cell harvest was performed as previously described.[21] Twenty-four hours after inhibitor treatment, culture medium was removed, and cells were washed two times with ice cold PBS. Mammalian Protein Extraction Reagent (M-PER) buffer (Pierce) containing protease inhibitor cocktail III (Calbiochem), 100 mM phenylmethylsulfonyl fluoride (PMSF), and phosphatase inhibitor II and III mixtures (Sigma) were added to washed cells at a 1:100 dilution and scraped. Scraped cells in lysis buffer were incubated for 10 min on ice to allow for lysis to occur. Cell lysates were then centrifuged at 16 000*g* for 10 min to separate cell lysates from nuclear debris. Bicinchoninic acid assay (BCA) was performed to determine

DOI: 10.1021/acschembio.6b00747
ACS Chem. Biol. XXXX, XXX, XXX−XXX

protein concentration in cell lysates, and samples were prepared for Western blot analysis.

Western Blotting. Western blot analysis was performed as previously described.[41] Cell lysates were prepared at identical protein concentrations, as determined by BCA analysis, in 2× Laemmli sample buffer (Bio-Rad) and denatured by boiling for 5 min at 100 °C. Denatured samples were then loaded onto a 10-well 10% gel (Bio-Rad). Gels were run at 125 V until the dye front reached the bottom of the gel cassette. Gels were then transferred onto a PVDF membrane (Millipore) at 100 V for 1 h. After transfer, blots were blocked in 7% milk in TBS for 1 h at RT prior to primary antibody incubation. Statistical analysis of imaged blots was performed with ImageJ analysis software (NIH).

Antibodies. Myocilin antirabbit primary antibody was provided by Dan Stamer at Duke University. Actin antimouse was purchased from Sigma-Aldrich. Secondary antibodies were purchased from Southern Biotech. All antibodies were diluted at 1:1000 in 7% milk in TBS. Primary antibodies were incubated shaking overnight at 4 °C. Secondary antibodies were incubated shaking at RT for 1 h.

■ ASSOCIATED CONTENT

Supporting Information

The Supporting Information is available free of charge on the ACS Publications website at DOI: 10.1021/acschembio.6b00747.

Synthetic procedures, characterization data, ^{1}H and ^{13}C NMR spectra for **5a** and **8j** (PDF)

■ AUTHOR INFORMATION

Corresponding Author

*E-mail: bblagg@ku.edu.

ORCID

Brian S. J. Blagg: 0000-0002-6200-3480

Notes

The authors declare the following competing financial interest(s): The authors, with the exception of Suman Gosh, are coinventors of a patent based on this work.

■ ACKNOWLEDGMENTS

We would like to thank Heather Shinogle from the Microscopy and Analytical Imaging Laboratory at The University of Kansas for assistance with confocal imaging. This research was supported by grants CA109265 (B.S.J.B.) and EY024232 (B.S.J.B. and C.A.D.) from The National Institutes of Health (NIH). NMR instrumentation was supported by NIH Shared Instrumentation Grants (S10OD016360, S10RR024664) and an NSF Major Research Instrumentation Grant (0320648).

■ ABBRIVIATIONS USED

SBDD, structure-based drug design; GARP, glycoprotein-A repetitions predominant protein; DPPF, 1,10-bis-(diphenylphosphino)ferrocene; LRP6, low-density lipoprotein receptor-related protein 6; LG, leaving group; RT, room temperature

■ REFERENCES

(1) Taipale, M., Jarosz, D. F., and Lindquist, S. (2010) HSP90 at the hub of protein homeostasis: emerging mechanistic insights. *Nat. Rev. Mol. Cell Biol. 11*, 515−528.

(2) Trepel, J., Mollapour, M., Giaccone, G., and Neckers, L. (2010) Targeting the dynamic HSP90 complex in cancer. *Nat. Rev. Cancer 10*, 537−549.

(3) Khandelwal, A., Crowley, V. M., and Blagg, B. S. (2016) Natural product inspired N-terminal Hsp90 inhibitors: from bench to bedside? *Med. Res. Rev. 36*, 92−118.

(4) Jarosz, D. (2016) Hsp90: A Global Regulator of the Genotype-to-Phenotype Map in Cancers. *Adv. Cancer Res. 129*, 225−47.

(5) Whitesell, L., Bagatell, R., and Falsey, R. (2003) The stress response: implications for the clinical development of Hsp90 inhibitors. *Curr. Cancer Drug Targets 3*, 349−358.

(6) Calderwood, S. K., and Gong, J. (2016) Heat Shock Proteins Promote Cancer: It's a Protection Racket. *Trends Biochem. Sci. 41*, 311−23.

(7) Zhang, H., and Burrows, F. (2004) Targeting multiple signal transduction pathways through inhibition of Hsp90. *J. Mol. Med. 82*, 488−499.

(8) Pearl, L. H., and Prodromou, C. (2000) Structure and in vivo function of Hsp90. *Curr. Opin. Struct. Biol. 10*, 46−51.

(9) Prodromou, C., and Pearl, L. H. (2003) Structure and functional relationships of Hsp90. *Curr. Cancer Drug Targets 3*, 301−323.

(10) DeBoer, C., Meulman, P. A., Wnuk, R. J., and Peterson, D. H. (1970) Geldanamycin, a new antibiotic. *J. Antibiot. 23*, 442−7.

(11) Whitesell, L., Mimnaugh, E. G., De Costa, B., Myers, C. E., and Neckers, L. M. (1994) Inhibition of heat shock protein HSP90-pp60v-src heteroprotein complex formation by benzoquinone ansamycins: essential role for stress proteins in oncogenic transformation. *Proc. Natl. Acad. Sci. U. S. A. 91*, 8324−8.

(12) Bhat, R., Tummalapalli, S. R., and Rotella, D. P. (2014) Progress in the discovery and development of heat shock protein 90 (Hsp90) inhibitors. *J. Med. Chem. 57*, 8718−28.

(13) Sidera, K., and Patsavoudi, E. (2014) HSP90 inhibitors: current development and potential in cancer therapy. *Recent Pat. Anti-Cancer Drug Discovery 9*, 1−20.

(14) Jhaveri, K., Taldone, T., Modi, S., and Chiosis, G. (2012) Advances in the clinical development of heat shock protein 90 (Hsp90) inhibitors in cancers. *Biochim. Biophys. Acta, Mol. Cell Res. 1823*, 742−755.

(15) Peterson, L. B., Eskew, J. D., Vielhauer, G. A., and Blagg, B. S. (2012) The hERG channel is dependent upon the Hsp90α isoform for maturation and trafficking. *Mol. Pharmaceutics 9*, 1841−1846.

(16) Subbarao Sreedhar, A., Kalmar, E., Csermely, P., and Shen, Y. F. (2004) Hsp90 isoforms: functions, expression and clinical importance. *FEBS Lett. 562*, 11−15.

(17) Kozutsumi, Y., Segal, M., Normington, K., Gething, M., and Sambrook, J. (1988) The presence of malfolded proteins in the endoplasmic reticulum signals the induction of glucose-regulated proteins. *Nature 332*, 462−464.

(18) Li, Z., and Srivastava, P. K. (1993) Tumor rejection antigen gp96/grp94 is an ATPase: implications for protein folding and antigen presentation. *EMBO J. 12*, 3143−51.

(19) Goodman, S. L., and Picard, M. (2012) Integrins as therapeutic targets. *Trends Pharmacol. Sci. 33*, 405−412.

(20) Dejeans, N., Glorieux, C., Guenin, S., Beck, R., Sid, B., Rousseau, R., Bisig, B., Delvenne, P., Buc Calderon, P., and Verrax, J. (2012) Overexpression of Grp94 in breast cancer cells resistant to oxidative stress promotes high levels of cancer cell proliferation and migration: implications for tumor recurrence. *Free Radical Biol. Med. 52*, 993−1002.

(21) Suntharalingam, A., Abisambra, J. F., O'Leary, J. C., III, Koren, J., III, Zhang, B., Joe, M. K., Blair, L. J., Hill, S. E., Jinwal, U. K., Cockman, M., Duerfeldt, A. S., Tomarev, S., Blagg, B. S., Lieberman, R. L., and Dickey, C. A. (2012) Glucose-regulated protein 94 triage of mutant myocilin through endoplasmic reticulum-associated degradation subverts a more efficient autophagic clearance mechanism. *J. Biol. Chem. 287*, 40661−40669.

(22) Gullo, C. A., and Teoh, G. (2004) Heat shock protein: to present or not, that is the question. *Immunol. Lett. 94*, 1−10.

(23) Obeng, E. A., Carlson, L. M., Gutman, D. M., Harrington, W. J., Lee, K. P., and Boise, L. H. (2006) Proteasome inhibitors induce a terminal unfolded protein response in multiple myeloma cells. *Blood 107*, 4907−4916.

DOI: 10.1021/acschembio.6b00747
ACS Chem. Biol. XXXX, XXX, XXX−XXX

(24) Hua, Y., White-Gilbertson, S., Kellner, J., Rachidi, S., Usmani, S. Z., Chiosis, G., DePinho, R., Li, Z., and Liu, B. (2013) Molecular chaperone gp96 is a novel therapeutic target for multiple myeloma. *Clin. Cancer Res. 19*, 6242−6251.
(25) Chen, B., Piel, W. H., Gui, L., Bruford, E., and Monteiro, A. (2005) The HSP90 family of genes in the human genome: insights into their divergence and evolution. *Genomics 86*, 627−637.
(26) Soldano, K. L., Jivan, A., Nicchitta, C. V., and Gewirth, D. T. (2003) Structure of the N-terminal domain of Grp94. Basis for ligand specificity and regulation. *J. Biol. Chem. 278*, 48330−48338.
(27) Cristalli, G., Lambertucci, C., Taffi, S., Vittori, S., and Volpini, R. (2003) Medicinal chemistry of adenosine A2A receptor agonists. *Curr. Top. Med. Chem. 3*, 387−401.
(28) Immormino, R. M., Metzger, L. E., Reardon, P. N., Dollins, D. E., Blagg, B. S., and Gewirth, D. T. (2009) Different poses for ligand and chaperone in inhibitor-bound Hsp90 and Grp94: implications for paralog-specific drug design. *J. Mol. Biol. 388*, 1033−1042.
(29) Patel, P. D., Yan, P., Seidler, P. M., Patel, H. J., Sun, W., Yang, C., Que, N. S., Taldone, T., Finotti, P., Stephani, R. A., Gewirth, D. T., and Chiosis, G. (2013) Paralog-selective Hsp90 inhibitors define tumor-specific regulation of HER2. *Nat. Chem. Biol. 9*, 677−684.
(30) Duerfeldt, A. S., Peterson, L. B., Maynard, J. C., Ng, C. L., Eletto, D., Ostrovsky, O., Shinogle, H. E., Moore, D. S., Argon, Y., Nicchitta, C. V., and Blagg, B. S. J. (2012) Development of a Grp94 inhibitor. *J. Am. Chem. Soc. 134*, 9796−9804.
(31) Crowley, V. M., Khandelwal, A., Mishra, S., Stothert, A. R., Huard, D. J. E., Zhao, J., Muth, A., Duerfeldt, A. S., Kizziah, J. L., Lieberman, R. L., Dickey, C. A., and Blagg, B. S. J. (2016) Development of Glucose Regulated Protein 94-Selective Inhibitors Based on the BnIm and Radamide Scaffold. *J. Med. Chem. 59*, 3471−3488.
(32) Ernst, J. T., Liu, M., Zuccola, H., Neubert, T., Beaumont, K., Turnbull, A., Kallel, A., Vought, B., and Stamos, D. (2014) Correlation between chemotype-dependent binding conformations of HSP90α/β and isoform selectivity—Implications for the structure-based design of HSP90α/β selective inhibitors for treating neurodegenerative diseases. *Bioorg. Med. Chem. Lett. 24*, 204−208.
(33) Gilow, H., and Burton, D. (1981) Bromination and chlorination of pyrrole and some reactive 1-substituted pyrroles. *J. Org. Chem. 46*, 2221−2225.
(34) Chen, W., Stephenson, E. K., Cava, M. P., and Jackson, Y. A. (1992) 2-Substituted Pyrroles from N-tert-Butoxycarbonyl-2-Bromopyrrole: N-tert-Butoxycarbonyl-2-Trimethylsilylpyrrole. *Org. Synth. 70*, 151.
(35) Chakrabarty, M., Kundu, T., and Harigaya, Y. (2006) Mild Deprotection Of Tert -Butyl Carbamates Of NH-Heteroarenes Under Basic Conditions. *Synth. Commun. 36*, 2069−2077.
(36) Bohm, H. J., Banner, D., Bendels, S., Kansy, M., Kuhn, B., Muller, K., Obst-Sander, U., and Stahl, M. (2004) Fluorine in medicinal chemistry. *ChemBioChem 5*, 637−43.
(37) Ghosh, S., Shinogle, H. E., Galeva, N. A., Dobrowsky, R. T., and Blagg, B. S. J. (2016) Endoplasmic Reticulum Resident Heat Shock Protein 90 (Hsp90) Isoform Glucose-Regulated Protein 94 (Grp94) Regulates Cell Polarity and Cancer Cell Migration by Affecting Intracellular Transport. *J. Biol. Chem. 291*, 8309−8323.
(38) Rachidi, S., Sun, S., and Li, Z. (2015) Endoplasmic reticulum heat shock protein gp96/grp94 is a pro-oncogenic chaperone, not a tumor suppressor. *Hepatology 61*, 1766−1767.
(39) Mattila, P. K., and Lappalainen, P. (2008) Filopodia: molecular architecture and cellular functions. *Nat. Rev. Mol. Cell Biol. 9*, 446−454.
(40) Wang, N., Feng, Y., Lau, E. P., Tsang, C., Ching, Y., Man, K., Tong, Y., Nagamatsu, T., Su, W., and Tsao, S. (2010) F-actin reorganization and inactivation of rho signaling pathway involved in the inhibitory effect of Coptidis Rhizoma on hepatoma cell migration. *Integr. Cancer Ther. 9*, 354−64.
(41) Stothert, A., Suntharalingam, A., Huard, D., Fontaine, S., Crowley, V., Mishra, S., Blagg, B., Lieberman, R., and Dickey, C. (2014) Exploiting the interaction between Grp94 and aggregated myocilin to treat glaucoma. *Hum. Mol. Genet. 23*, 6470−80.
(42) Okado-Matsumoto, A., and Fridovich, I. (2001) Subcellular distribution of superoxide dismutases (SOD) in rat liver: Cu,Zn-SOD in mitochondria. *J. Biol. Chem. 276*, 38388−93.

DOI: 10.1021/acschembio.6b00747
ACS Chem. Biol. XXXX, XXX, XXX−XXX